N and *Z* dependence of nuclear charge radii

2009 J. Phys. G: Nucl. Part. Phys. 36 085102

(http://iopscience.iop.org/0954-3899/36/8/085102)

J. Phys. G: Nucl. Part. Phys. **36** (2009) 085102 (26pp) doi:10.1088/0954-3899/36/8/085102

N and *Z* dependence of nuclear charge radii

I Angeli[1], Yu P Gangrsky[2], K P Marinova[2], I N Boboshin[3], S Yu Komarov[3], B S Ishkhanov[3] and V V Varlamov[3]

[1] Institute of Experimental Physics, University of Debrecen, H-4010 Debrecen, Pf 105, Hungary
[2] Joint Institute for Nuclear Research, 141980 Dubna, Moscow Region, Russia
[3] Skobeltsyn Institute of Nuclear Physics, Lomonosov Moscow State University, 119991 Moscow, Russia

E-mail: angeli@tigris.klte.hu and marinova@nrmail.jinr.ru

Received 27 January 2009
Published 8 June 2009
Online at stacks.iop.org/JPhysG/36/085102

Abstract

This paper is devoted to the analysis of the general trends in the nucleon number dependence of the experimental root-mean-square (rms) charge radii. It is based on the data obtained by different methods of combined treatment of (i) radii changes determined from optical and—to a lesser extent—K_αx-ray isotope shifts, and (ii) absolute radii measured from muonic and electronic scattering experiments. These methods have recently been developed and now updated including experimental data up to the beginning of 2008. Thus, new sets of rms nuclear radii have been obtained covering 865 isotopes for 76 elements from $_1$H to $_{96}$Cm. New information on the isotopic and isotonic behaviour of the nuclear charge radius is obtained with a high accuracy compared to that of the directly measured radii values for the same element. Of special interest is that concerning the light elements and the appearance of non-traditional magic neutron and proton numbers, as $N = 6$, 14 and $Z = 14$; the double-magic properties of ^{96}Zr are discussed in more detail. A quantitative criterion is introduced, which points to the peculiarities in the radii trend and offers an opportunity to investigate it more closely. The results provide important information which may serve as a guide to incorporate essential new features into the theoretical approaches.

(Some figures in this article are in colour only in the electronic version)

1. Introduction

The nuclear root-mean-square (rms) charge radius $R = \langle r^2 \rangle^{1/2}$ is a fundamental property of atomic nuclei. It can be measured by methods based on the electromagnetic interaction between the nucleus and electrons or muons. Four methods are known: measurements of transition energies in muonic atoms (μ^-), elastic electron scattering experiments (e^-),

K_αx-ray and optical isotope shifts (KIS, OIS). The first two supply information on R, and the latter ones on their isotopic changes $\delta\langle r^2\rangle$. Experiments with μ^- atoms, electron scattering and K_αx-rays have been performed only on stable isotopes since those require several tens of milligrams of a target material. The optical laser spectroscopy gives access to measurements of micro quantities of radioactive atoms with lifetimes down to 1 ms. In the last decade, sophisticated laser methods have been developed, often combined with storage techniques of different kind, which are able to work even with single atoms (ions) and have extended our knowledge on nuclei *far from stability*. Both groups of experimental methods are complementary: combining the data on the rms radii R of a stable reference isotope A' with the radius change $\delta\langle r^2\rangle^{A'A} = \langle r^2\rangle^A - \langle r^2\rangle^{A'}$ between A' and a radioactive isotope A, one can find the $R(A)$-value of any isotope A in a long isotopic sequence using the simple relation

$$R^2(A) = R^2(A') + \delta\langle r^2\rangle^{A'A}. \tag{1}$$

In fact, the problem is more complicated than it seems. This is due to many factors. The most precise nuclear R-values have been obtained by use of the muonic atom spectroscopy, the precision being limited by the uncertainties of the calculated nuclear polarization corrections. Muonic spectra measure radial moments which depend explicitly on the particular muonic transition and differ significantly from $\langle r^2\rangle$ except for the lightest elements. Nevertheless, the systematic behaviour of the isotopic and isotonic shifts for the stable isotopes could be determined using experiments with muonic atoms. Electron scattering experiments offer an alternative access to nuclear charge radii through the form factor, providing an excellent model-independent determination of $\langle r^2\rangle$. However, the precise measurement of small $\delta\langle r^2\rangle$ effects in isotopic series is difficult and has been performed only in a limited number of cases. Let us note that R-values from μ^- and e^- measurements are often significantly different; moreover, the data of different authors using one and the same experimental method have shown essential spread (see e.g. [1]). Laser spectroscopy yields optical isotope shifts with very high accuracy (often only tenths of a percent), but in deducing $\delta\langle r^2\rangle^{A'A}$ one has to determine the electronic factor F for the optical transition and the mass shift part M_S of the isotope shift. Various ways used to get the F- and M_S-values may provide slightly different slopes of $\delta\langle r^2\rangle^{A'A}$ and consequently of the R curves. In the case of K_αx-ray isotope shifts, the nuclear charge distribution investigated is the same as in the optical isotope shifts; the evaluation of $\delta\langle r^2\rangle^{A'A}$ is straightforward, but the experimental uncertainties are too large and hamper the calibration of optical isotope shifts via K_αx-ray data. Thus, a very careful and critical analysis of the data has to be performed and its results have been discussed before using equation (1) for a combined evaluation of different types of experimental data to derive R-values in long isotopic chains.

Nowadays, three different methods for the combined analysis of both types of experimental data, on R and on $\delta\langle r^2\rangle$, are suggested [2–4]. These are not simple compilations of individual measurements, but contain self-consistent sets of R-values.

The present paper aims to study the general trends in the nucleon number dependence of the experimental rms charge radii. The work is motivated to a great extent by the possibility of analysing the behaviour not only of the isotopic but also of the isotonic radii sequences over the whole nuclide chart. Of great importance in this aspect are the new data obtained in the region of light nuclei. A quantitative criterion is introduced, which describes the peculiarities in the radii trend and offers an opportunity to investigate it in more detail. The strong dependence of charge radii on the proton number gives insight into the general characteristics of radii development and is influenced only a little by the specific details of the nuclear structure. On the other hand, the essentially weaker radius dependence on the neutron number enables

revealing even a slight influence of different nuclear parameters, e.g. deformation, moments, energy of nucleon pairing.

The paper is based on the data of [5, 6], which are the updated and modified versions of [2, 3], containing the rms nuclear charge radii of 865 isotopes of 76 elements from $_1$H to $_{96}$Cm. These are at present the most complete collection of the experimental data giving a global survey of the charge radii in extended ranges of Z and N: $1 \leqslant Z \leqslant 96$ and $0 \leqslant N \leqslant 152$. The full tables are accessible online and can be found in the database of the Lomonosov Moscow State University, Skobeltsyn Institute of Nuclear Physics [7].

In section 2, the general principles (algorithms) of the methods of combined analysis of R and $\delta\langle r^2\rangle$ data are summarized and some comments concerning the results are given. A major part of the paper is devoted to the description and analysis of the present status of isotopic and isotonic behaviour of the nuclear charge radii—sections 3 and 4, respectively. In section 5, experimental and theoretical results are compared and briefly discussed.

2. Combined analysis of optical and non-optical data

Nadjakov *et al* [2] suggested a least-squares fit procedure for both types of data, rms radii R and ms charge radii changes $\delta\langle r^2\rangle$, based on equation (1). The updated values of nuclear charge radii [6] differ strongly from those in [2] due to changed input data. The main source for the R-values is the table of [1] which summarizes data from a large number of e^- and μ^- experiments. The few exceptions are displayed in the reference list (see [6]). Original papers on optical isotope shifts instead of review papers are used and treated with the necessary precaution. In the procedure of extracting the nuclear parameter λ, the semi-empirical approach using optical information was preferred whenever possible. Experimental λ were converted into $\delta\langle r^2\rangle$-values using the corrections for the higher order radial moments given by [4]. References for the input data on $\delta\langle r^2\rangle$ are given for each isotope in the table [7].

The data sources and treatment of the tables [3] have been described in detail in [1] for the R-values, while in [3] the treatment of differences δR is given. The sources for radii changes $\delta\langle r^2\rangle$ are the original papers (see [3, 5]). For absolute R-values, experimental data from electron scattering (e^-), muonic atom x-rays (μ^-) as well as the Lamb shift (for the proton) were taken into account. For differences δR, in addition to e^- and μ^-, data from K_α isotope shifts (KIS) and optical isotope shifts (OIS) were used. Constraints between δR- and R-values were exploited wherever possible. In the new version [5], there are three important changes: 66 new data points were added, several old data were corrected using more recent information and a change in the evaluation procedure of absolute R radii from e^- and μ^- was performed. These latter changes are small—in general, they do not exceed the errors—but they refer to most of the R data.

The model-independent method proposed by Fricke *et al* [4, 8] is based on the simultaneous calibration of the electronic factor F and mass shift M_S using the King plot [9] of optical isotope shift data versus $\delta\langle r^2\rangle$-values extracted from isotope shift measurements in muonic atoms. Additional electron scattering experiments have been used to obtain the radial dependence of the charge distribution and to extract the charge radius from the very precise and model-independent Barrett radius obtained in muonic atom experiments. Due to the lack of electron scattering data, this combined analysis cannot be used for all isotope series. Many of the numerical values are presented without error estimation.

In all the three cases, the combined treatment is applicable to those elements for which both types of data exist. The differences in the absolute R-values between these data sets are usually less than or around 1%, see also [10]. Although small, these differences lead to unexpected charge radii behaviour in some cases of [4]. Figures 1 and 2 show two examples.

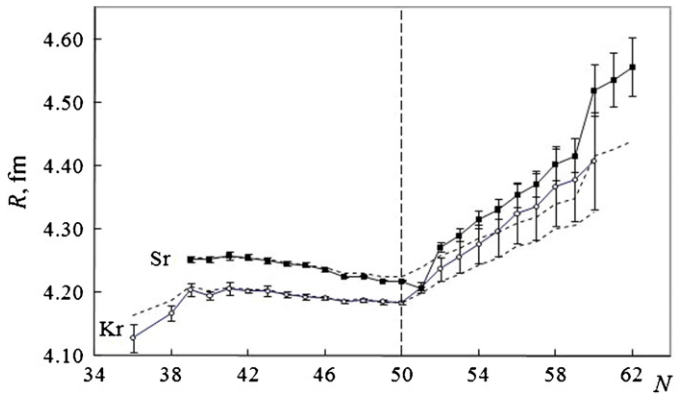

Figure 1. Charge radii evolution in Kr (open circles) and Sr (full squares) according to [4]. For comparison, the radii trend predicted from [6] (dashed lines) is shown too. For Kr the data of [5, 6] coincide in the fourth digit; this is also the case for Sr in the neutron region $N \leqslant 50$. Above $N = 50$, the R-values from [5] lie in between those of [4, 6].

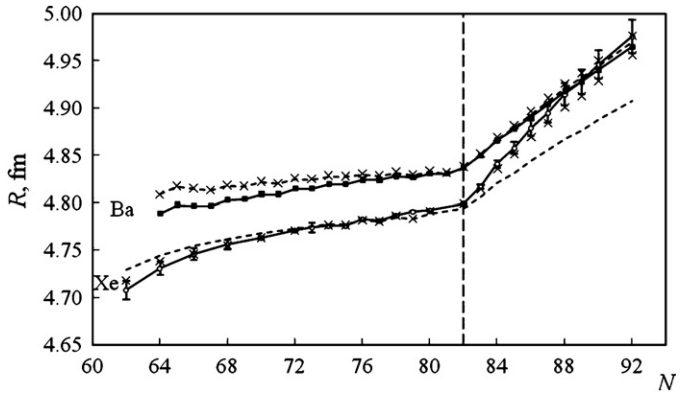

Figure 2. Charge radii evolution in Xe (open circles) and Ba (full squares) according to [4] compared to those evaluated by [6] (dashed lines) and [5] (crosses). The R-values of Xe [5] lie in between those of [4, 6] and do not lead to a intersection of both curves—Ba and Xe.

The radii trend [4] of Kr and Sr (figure 1) does not show the very similar evolution of $\delta\langle r^2\rangle$ for both isotopic chains, as obtained and discussed in [11–13]. The sudden decrease of the strontium radius at $N = 51$ predicted by [4] cannot find a reasonable explanation from the point of view of the nuclear deformation (see [11]). A crossing of the Xe and Ba isotopic curves (figure 2) follows from [4] while in the semi-empirical radii evaluation from OIS, the curves run parallel to each other (see [14] and references therein) and are in a quantitative agreement with deformation parameters derived from the spectroscopic quadrupole moments or the $B(E2)$-values. This is exactly the case of the data [6] and with a good approximation of [5].

Different reasons may be responsible for such discrepancies. The most obvious is connected with the F factor (and specific mass shift especially in the case of light elements). Traditionally, $F = F_{\mathrm{SE}}$ is evaluated from atomic electron shell data using either semi-empirical procedures and/or Hartree–Fock calculations of the relevant electronic density at the site of the

nucleus. In some favourable cases, e.g. pure alkali-like s → p optical transitions, the accuracy of the semi-empirical calculations is within 1–3% [11, 13, 15]. Usually an error of the order 5–10% has been adopted [14]. The uncertainties of $F_{\mu e}$ quoted in the model-independent analysis [4] are about 13%. However, the differences between optical approximation and the values obtained in [4] are in some cases about 50%, e.g. this is the case of Sr.

The calibrations of the electronic factor and mass shift in [4] have been performed using the King plot for stable isotopes only. It is not obvious whether the results obtained in this way are unambiguously valid in the cases of long isotopic chains far off stability. The most serious discrepancies are observed for those elements whose stable isotopes, providing the muonic radii for the King plot, are located close to the magic numbers $N = 50$ and $N = 82$. In these particular cases, the muonic radii are nearly constant and the radii changes are very small. Therefore, the slightest error in the muonic IS will have dramatic consequences—in spite of the undoubtedly high precision of the absolute muonic Barrett moments. Thus, the $F_{\mu e}$-values cannot be enough precisely determined to get right R-values for the nuclei located far away from the magic number. Additional problem arises due to the corrections of the muonic R-values for the nuclear polarization. These corrections fluctuate only by a few percent up and down suggesting a nearly spherical nuclear shape, while a long isotopic chain can connect regions with very different nuclear structures. The problem is discussed in detail by Libert *et al* [10] for Xe and Ba (see figure 2). It is shown that in these cases the method proposed in [4] reaches its limits. Moreover, the theoretical description [10] of the charge radii accounting for dynamical deformation is in a better agreement with the experimental R-value of Xe and Ba obtained by semi-empirical analysis than with the model-independent data of [4].

The situation is different in the vicinity of the magic number $N = 126$. The King plot in [4] is not affected by the deformation because the stable isotopes of Hg and Pb [16] are near spherical. In this (N, Z) region the results of [4], [5] and [6] are in very good agreement.

In the following, we lay stress on several important peculiarities of the radii trend over the whole nuclear chart. It is worth noting that the general trends of the charge radii over the whole nuclide chart have the same fundamental peculiarities in the three data sets, the closest being the data of [5, 6]. As the aim of this paper is to investigate the *trends* in the nucleon number dependence of rms charge radii—rather than to produce 'best values' for individual nuclei—in all the following figures, the averaged R-values from [5, 6] are plotted. The differences between them are usually essentially less than 1% and do not affect the general picture. Readers who are looking for $R(\pm\Delta R)$-values for specific nuclides may consult the individual numerical data in [4–6]. In this way, they can get an estimate of the uncertainty caused by the different evaluation procedures.

3. Isotopic rms radii behaviour

The isotopic dependence of nuclear charge radii, expressed in terms of radii changes $\delta\langle r^2\rangle$, has been an object of a huge number of papers and has been discussed many times (see e.g. the reviews [14, 17]). Transforming $\delta\langle r^2\rangle$ into absolute rms radii values, one receives a global overlook on the isotopic charge radii trend over the whole nuclide chart. On average, a smooth mass number dependence

$$R_Z(A) = R_0\left(\frac{A}{A_0}\right)^{1/6} \tag{2}$$

was obtained (see [3], figure 2, table 3), where R_0 is the rms charge radius of the reference isotope (Z, A_0) and $R_Z(A)$ denotes radii at the constant Z. This weak A dependence is due to

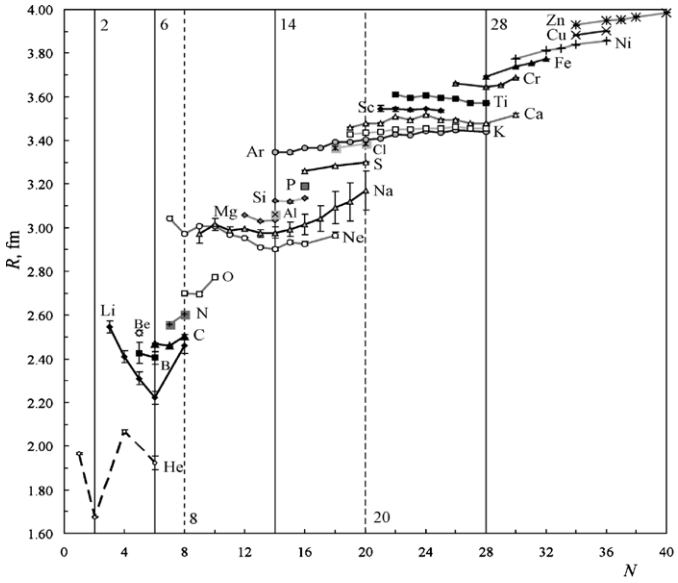

Figure 3. Isotopic behaviour of rms charge radii for the light elements from $_2$He to $_{30}$Zn. For the sake of completeness, cases in which the *R*-data result only from non-optical measurements are also shown [5]. In this and all cases below the error bars include the total, statistical plus systematic, uncertainties of the input data, as given in [5] (in [6] the uncertainties are underestimated).

the fact that along the isotopic chain of an element only the neutron number varies, while the charge Ze remains constant. More detailed investigations [18] have shown that the exponent in equation (2) is an increasing function of Z: $k_Z \approx 0.003 \times Z$; for the definition of k_Z see equation (9) in [3].

For individual elements, however, there are significant local variations owing to shell and deformation effects. The *status quo* is displayed in figures 3 and 4. We will concentrate the attention on the following aspects of the data: magic numbers, deformations, similarity between the successive curves, *normal* odd–even staggering and data reliability.

3.1. The second difference of $R_Z(N)$ as a tool for structure search

Besides simply inspecting the radius data along an isotopic series R_Z (N), the search for deviations from the smooth neutron number dependence can be made easier and *quantitative* by the investigation of the second differences; this is a well-known mathematical method applied in physics too. Based upon this, the slope change can be characterized by the value of the kink strength S (see the appendix). The numerical value of this quantity may play a similar role in investigating isotopic series as the Brix–Kopfermann plot (see [19], figure 84; [14], figure 44) or as the value of level energies in individual nuclei. Odd–even effects are eliminated by taking the differences with a basis length $\Delta N = 2$.

As examples, the magic neutron number $N_M = 50$ has a strength $S = 0.75(1)$ fm in Kr and $S = 0.95(1)$ fm in Rb, Sr and Zr alike, while $N_M = 82$ has values between $S = 0.61$ and 0.77 fm in the series of Xe, Cs, Ba, Ce, Nd, Eu and Dy. For $N_M = 126$ in Pb the kink strength is significantly lower: $S = 0.31(3)$ fm; this may be due to the stabilizing effect of the magic proton number $Z = 82$ (see [14], chapter 4.7.3).

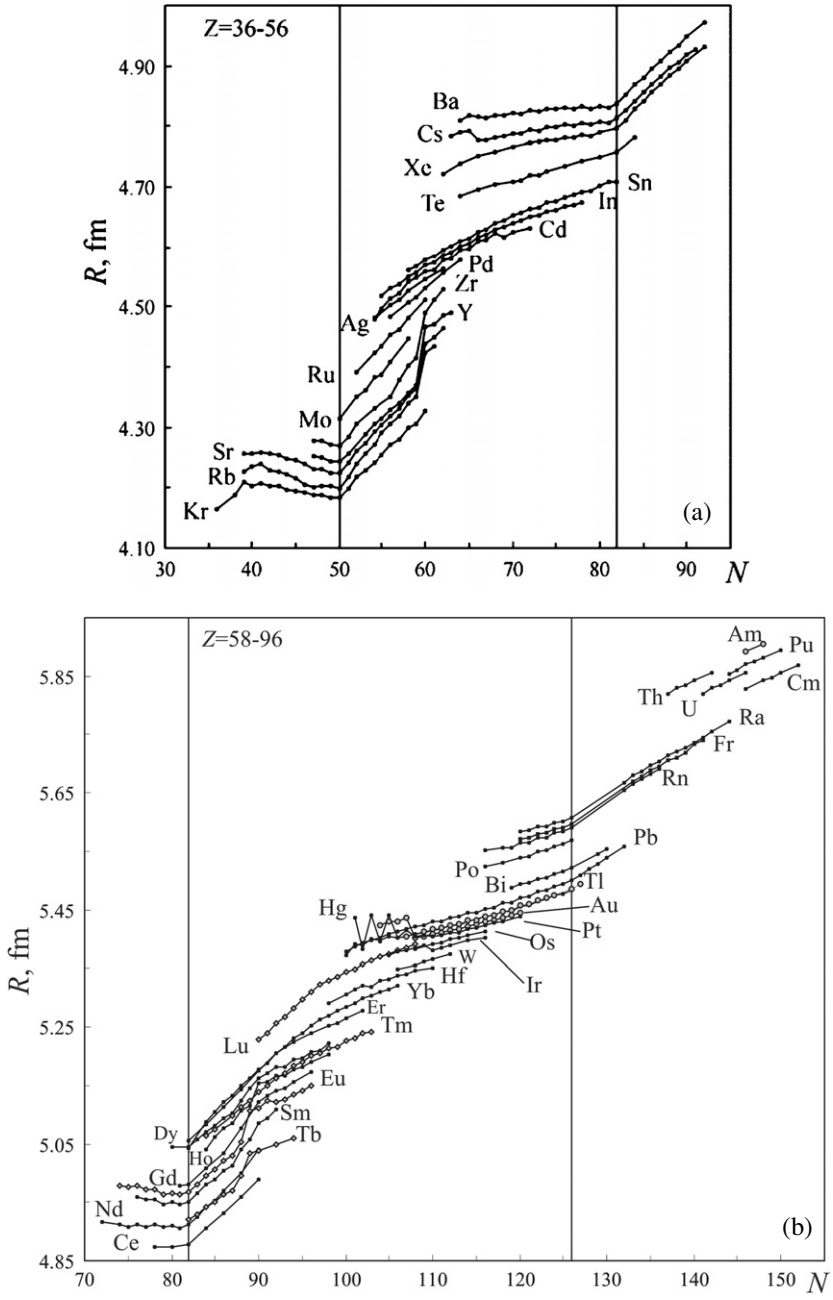

Figure 4. Isotopic behaviour of rms charge radii: (a) intermediate mass elements from $_{36}$Kr to $_{56}$Ba and (b) rare earths and heavy elements from $_{58}$Ce to $_{96}$Cm. Also elements are included for which neither μ^- nor e^- experimental data on R are available (Po, Rn, Fr, Ra and Cm). Reference radii R' for an appropriately chosen isotope in the isotopic sequences of these elements are calculated by equation (22) of [1] using the parameters of [5].

Shell closures are always characterized with positive S-values, while deformation changes may produce both positive and negative curvatures. A classic example of shape transition is $^{152}Eu_{89}$, and this is verified by a very high negative S-value: $S = -1.73(23)$ fm. For more detailed information see the following sections, as well as table A1 and figure A1(d) in the appendix.

3.2. Series of light elements

The effect of magic neutron numbers and large, permanent deformations has been recognized long ago (see [20], figure 6; [21], figures 1 and 2; [2], figure 1). The shell closure effect on the charge radii manifests itself in characteristic slope changes of radii at magic neutron numbers N_M and is well pronounced at all neutron shell closures with $N \geqslant 28$ (see figures 3 and 4). In this context, the region of light elements (figure 3) deserves closer consideration.

The conventional neutron magic numbers in this region are $N_M = 2$, 8, 20 and 28. The shell effect in the radii development is clearly seen only at $N_M = 28$: $S(^{48}Ca_{28}) = 0.76(7)$ fm and $S(^{52}Cr_{28}) = 0.87(8)$ fm. The situation for lower neutron numbers is drastically changed. In the series of He, the radius shows an absolute minimum at $N = 2$, but the size of ^{8}He is also less than that of ^{3}He. This calls the attention to the role of $N = 6$. The high radius value of ^{6}He is probably due to the polarizing effect of the two *halo neutrons*. A characteristic kink in the isotopic curves for light nuclei arises at $N = 6$ and $N = 14$, instead at the conventional magic numbers $N = 8$ and $N = 20$. For example, the highest positive S-value is observed at $N = 6$ for Li: $S(^{9}Li_6) = 1.90(32)$ fm.[4]

The conventional shell closure $N = 8$ is crossed only by the neutron-deficient isotopes of Ne where a significant dip at $N = 8$ can be observed. However, because of some specific features in these cases, it cannot be decided if this dip is a real *slope change* caused by shell closure (cf figures A1(b) and (c) at $N = 50$ and 82), or some *local* effect. A large radius of even–odd ^{17}Ne has been measured [23]. This nucleus is widely discussed as a prominent candidate for two-proton halo [23–25] and its enhanced charge radius is attributed to a very large $\pi 2s^2$ component of the two-proton ground state.

Isotope shifts of Na and Ne isotopes indicated the magic-like behaviour at neutron number $N = 14$ (see [26], figures 11 and 12]), corresponding to the closure of the $d_{5/2}$ subshell [27]; here the kink strengths are $S(^{24}Ne) = 0.63(7)$ fm and $S(^{25}Na) = 0.46(10)$ fm. In addition, there is also a small dip at $N = 16$ with $S = 0.11(8)$ fm. This behaviour is in agreement with the available data on the quadrupole deformation, especially in the case of neon. Although the neon isotopes from the sd shell are strongly deformed, ^{24}Ne has the least quadrupole deformation as compared to its even–even neighbours [28]. Moreover, the observed peculiarity is in accordance with the systematics of the energy of the first excited states in the $Z = 10$ isotopic sequence: $E(2^+)$ reaches a maximum value around ν2s1d mid-shell, at $N = 14$, 16 [29]. A more detailed experimental and especially theoretical study of the ground-state properties of Ne and Na isotopes is obviously necessary.

On the other hand, what is seen in figure 3 is in favour of disappearance of the $N = 20$ magicity. The experimental data on the *charge radii* trend around $N = 20$ cover two different Z regions: (i) neutron-rich nuclei from the ν2s1d shell of elements around $Z = 10$ and (ii) nuclei from the $\nu 1f_{7/2}$ shell around $Z = 20$ (the Ca region). For case (i), the effect was first demonstrated for ^{31}Na by [26 and 27]. Subsequent observations revealed a region of *deformation* around the $N = 20$ isotones—^{31}Na [30], ^{30}Ne [31] and ^{32}Mg [32]. The divergence between shell model calculations in the νsd shells and observed properties of neutron-rich Ne, Na, and Mg isotopes was ascribed [33] to the inversion of the spherical closed-shell

[4] The recent OIS data on $^{7,9-11}$Be [22] show an analogous radii trend as for Li.

configurations and the deformed multiparticle-multihole (ph) intruder configurations. Thus, the region is known as the 'island of inversion'.

As pointed out in [34–36], the most striking characteristic of nuclei from the Ca region (Ar, K and Ca) is that the conventional magic number $N = 20$ has no visible influence on the development of charge radii. It increases smoothly across $N = 20$ without showing the usual shell effect. However, it should be stressed that there is still no quantitative confirmation of this statement by means of the S-value. In the cases of K and Ca, the kink strength at $N = 20$ cannot be calculated because no data on rms charge radii of even-N isotopes below the neutron shell closure $N = 20$ are available. Although for ^{38}Ar the S-value is significantly positive, $S = 0.14(2)$ fm is much smaller than those found for $N_M \geqslant 28$, while as a rule it should be larger for lighter nuclei. $N = 20$ isotopes of these elements are stable, ^{40}Ca is a well-known double magic nucleus and many of the ^{38}Ar and ^{39}K characteristics are consistent with the magicity of $N = 20$. Thus, this is a very different case compared to the one of the neutron-rich $10 \leqslant Z \leqslant 12$ isotopes. The absence of a visible shell effect in the nuclear radii trend at $N = 20$ is discussed in [34, 36] and explained by a cancellation of monopole and quadrupole polarization of the proton core under successive addition of valence neutrons.

It is interesting to have a look at *other experimental and theoretical results* which deal with the magic properties in the light nuclei region. Many scenarios exist and often the occurrence of new magic numbers and the disappearance of the conventional ones are still under discussion.

The earlier statistical study of deviations of rms charge radii—along the line of stability—from the droplet-model values in terms of the promiscuity factor P [37] has shown that $Z_M = 6$, 14 and $N_M = 8$, 14 should be taken into account as magic numbers, while $Z_M = 20$ and $N_M = 20$ should be disregarded (see [38], pp 442–5).

A recent systematics of the experimental energies of the *first excited* 2^+ *state* in light nuclei with $Z = 4$–24 has been published by Boboshin [39]. It is shown that in this region numerous deviations from the classical expected N and Z magic numbers are observed. Regions with increased $E(2_1^+)$-values appear at nucleon numbers which are not predicted by the shell model. This is e.g. the region for which the pair (Z, N) is either (6, 8) or (8, 6): the $E(2_1^+)$-value for these pairs is nearly the same as for the classical double magic nucleus ^{16}O. Many other nuclear properties of these nuclei are in favour of their magicity; it is worth noting that they have large quadrupole deformations, e.g. $\beta_2 = 0.364(17)$ for ^{16}O [28]. Nuclei with neutron or proton magic number 14 or 16 are other examples of non-traditional behaviour. The same refers to the neutron-rich nuclei in the vicinity of $Z = 8$ and $N = 14$, 16, and for $Z = 20$, 22 with $N = 32$, 34. The cancellation of the conventional magic numbers such as $N = 8$ [40, 41] and $N = 20$ [33] and the appearance of new magic numbers such as $N = 6$ and $N = 14$ or 16 in neutron-rich light nuclei have also been predicted theoretically [42, 43].

To sum up, the isotopic behaviour of nuclear charge radii for light elements ($3 \leqslant Z \leqslant 30$) is in favour of the magicity of $N = 6$ and $N = 14$, and contradicts or, at least, does not confirm that of $N = 8$ and $N = 20$. However, nuclei with $Z < 10$ are poorly investigated and the evidence of the shell effect in the charge radii and, thus, of appearance of new magic numbers is still not conclusive. A fuller picture necessitates extending the experimental information. Since the rms radii values for the stable isotopes in this Z region are already known, laser spectroscopic investigations of isotopic chains covering the neutron-rich isotopes of elements with $Z < 10$ would be of special importance. For example, a breakdown of $N = 8$ shell closure at ^{12}Be is not only predicted theoretically but also experimentally evidenced by inelastic proton scattering [40] and by one neutron knock-out reaction [41], respectively. Other interesting cases are the oxygen isotopes ^{22}O ($N = 14$) and ^{24}O ($N = 16$) both considered as doubly magic nuclei [44–46].

A continuation of the charge radii investigation across $N = 20$ for the isotopic series Ne, Na and Mg will reveal more details and provide a test for the available theoretical models.[5] With respect to the magicity of $N = 20$ for the elements of the Ca region, it is very important to study the nuclear radii development of K and Ca isotopic sequences deep towards the middle of the sd shell as it was done for Ar.

Although we concentrated the discussion on the magic numbers, there are two other effects which should be briefly mentioned. These are the behaviour of the successive isotopic curves and the odd–even staggering. The latter will be considered separately in section 3.4. As regards the shape, in general the neighbouring curves run nearly parallel. An exception is observed in the Ca region. Although some underlying parabolic dependence of charge radii on neutron number is evident for all four chains (Ar, K, Ca and Ti) [36], the differences between the isotonic neighbours are much greater than one might expect for such a restricted mass region. The curve shape for Ca is nearly a symmetric parabola. Away from the magic proton number, the parabola flattens out and an additional slope appears which is positive for $Z < 20$ and negative for $Z > 20$. The problem is pointed out and discussed in [36].

3.3. Series of intermediate and heavy elements

Figure 4 clearly illustrates the influence of the magic neutron numbers $N_M = 50$, 82 and 126 on the charge radii trend. The quantitative characteristics are given in section 3.1 and can be seen in table A1.

The formerly indicated similar features of the $R(N)$ curves for adjacent Z [2, 47] remains a general occurrence and is enriched with new peculiarities. These refer mainly to the isotopes far off stability. An example is the shape transition region at $N = 59$ (see [14] and the references therein). In addition to Rb [48] and Sr [11, 13], new data are available for the refractory elements Zr [49] and Y [50], all of them measured beyond $N = 60$ (figure 4(a)). The four curves run strongly parallel supporting the idea of competition between the various, coexisting nuclear shapes (well-deformed prolate, oblate and spherical). These shape changes are strongly reflected in the 'kink strength' value S for the neutron-rich isotopes with $N = 59$: $S(^{96}\mathrm{Rb}) = +1.18(8)$ fm, $S(^{97}\mathrm{Sr}) = +1.28(4)$ fm, $S(^{98}\mathrm{Y}) = +1.47(76)$ fm and $S(^{99}\mathrm{Zr}) = +1.48(3)$ fm, while for $N = 60$ a drastic sign change occurs, e.g. $S(^{98}\mathrm{Sr}) = -1.39(6)$ fm and $S(^{100}\mathrm{Zr}) = -1.19(3)$ fm.

The Cs isotopes with low mass numbers also deserve attention as suggested by their S-values for $N = 65$, 66 and 67: $S(^{120}\mathrm{Cs}) = -0.54(1)$ fm, $S(^{121}\mathrm{Cs}) = +0.43(2)$ fm and $S(^{122}\mathrm{Cs}) = +0.48(1)$ fm, respectively. These are in agreement with the deformation changes in the region of neutron-deficient cesium isotopes [51].

The kink at the magic neutron number $N = 82$ in Xe, Cs, Ba, Ce, Nd and Eu has already been mentioned in section 3.1, as well as the shape transition at $N = 89$ in connection with ^{152}Eu. It is worth to accent on the development of the negative kink strength values for $N = 90$: $S(^{152}\mathrm{Sm}) = -0.58(26)$ fm, $S(^{153}\mathrm{Eu}) = -1.41(2)$ fm, $S(^{154}\mathrm{Gd}) = -0.69(1)$ fm and $S(^{157}\mathrm{Ho}) = -0.91(2)$ fm. It follows exactly the trend of the maxima at $N = 90$ of the Brix–Kopferman plot in the rare-earth region (see [14], figure 44).

The region of shape coexistence for neutron-deficient nuclei around $Z = 80$ is extended with the data for a long Ir isotopic sequence [52] and additional information on very neutron deficient Au [53] and Pb [54] isotopes (figure 4(b)). The shape coexistence in neutron-deficient wings of isotopic chains from the Z region $Z = 77$–80 is reflected in the S-values showing abrupt changes not only in an absolute value but in sign too (see table A1 and figure A1(e) in the appendix).

[5] Such experiments are already in progress at the ISOLDE-CERN (http://isolde.web.cern.ch/ISOLDE/).

3.4. The normal odd–even staggering

The odd–even staggering (OES) is a phenomenon observed in practically all OIS experiments. However, this effect is in most cases disturbed by shell closure or deformation, resulting in values differing strongly not only in magnitude but also in sign: anomalous OES. Indeed, the different effects are not simply superimposed, but in some cases a strong interference between OES and deformation is observed, e.g. [16, 55, 56]: the pairing interaction 'triggers' the shape change. Experimental studies of the isotopic radii trend of different elements usually discuss this effect and there is a large amount of papers devoted to the OES of separated elements often in restricted isotopic chains. As regards the theory, it is shown [57] that with a suitable three-body part in the effective interaction, one is able to describe the OES of charge radii along isotopic series of Sn and Ba.

The consideration in this paper is of the context of revealing the general peculiarities of the charge radii over a broad range of N and Z. Therefore, in order to separate the *normal* OES from other disturbing effects, one has to select those 'quiet' regions of isotopic series that have low S-values, and are accurate enough to derive results usable by theory. The increased number and high relative accuracy of up-to-date rms charge radii rendered it possible to select such data. Results are summarized in table 1, where the weighted averages of the quantity

$$D_i = R_{i,\mathrm{odd}} - \tfrac{1}{2}(R_{i-1} + R_{i+1}) \tag{3}$$

are shown for the isotope regions and elements. Let us note that the nuclei in the neighbourhood of double magic ^{208}Pb provide favourable conditions to study the OES due to the reduced influence of the deformation effect [16, 58]. The OIS parameter D for Pb and Tl varies in nearly the same range as for Hg. These data are not included in table 1 because the full errors of D do not fulfil our criterion for statistical significance. It can be seen that the normal OES effect depends not only on the element, i.e. on the proton number, but also on the range of the neutron number. It is tempting to attribute the difference in range averages $\bar{D}_{\mathrm{range}}$ to the role of different neutron orbitals. The 'grand average' is $\bar{D}_{\mathrm{av}} = -2.49(17)$ am.

3.5. Effect of uncertainties

The main features of the isotopic radii systematics are insensitive to the uncertainties affecting only the overall scale of the $R(N)$-values. This is demonstrated in figure 5 for the Z region, where the isotopic curves are close together. A slight deviation from the similarity between the adjacent curves is observed in the neutron-deficient parts of Dy, Er and Yb isotopic chains, which are not resolved (figure 5(a)). The sharp jump of the charge radius in the shape transition region for rare earths as the neutron number changes from 88 to 90 is pronounced for $Z \leqslant 67$ (see figure A1(d) in the appendix), but the effect appears diminished for $_{68}$Er and essentially disappears for $_{70}$Yb [59], thus producing changes in the shape of the curves.

Many new data obtained in the last years, especially for the odd-Z elements, apparently modify the general picture and produce an uncommon crossover of the neighbouring curves. This holds not only for the rare-earth region shown in figure 5 but also for odd Z around $Z = 80$ at $100 \leqslant N \leqslant 110$ (figure 4(b)), both cases being shape transition regions. Note that the theoretical results of Goriely *et al* [60] based on the Hartree–Fock-BSC method (HFBSC-1) predict nearly similar behaviour around $Z = 80$.

Nevertheless, the resemblance of the subsequent curves remains. However, the large data uncertainties for Dy, Tb and Ho (see the caption of figure 5) imply some doubts about the plausibility of the absolute R-scale for these elements.

Table 1. Odd–even staggering parameters as defined by equation (3): $\bar{D}_{\text{range}}$ and $\bar{D}_{\text{el}}$ are the D-values, averaged over the neutron range or over an element, respectively.

Z	Element	A-range	N-range	D-range (am)	$\bar{D}_{\text{range}}$ (am)	$\bar{D}_{\text{el}}$ (am)
49	In	108–114	59–65	$-(1.9 \div 2.7)$	$-2.66(20)$	$-1.90(20)$
		116–122	67–73	$-(1.3 \div 1.6)$	$-1.37(16)$	
50	Sn	111–117	61–67	$-(1.0 \div 4.0)$	$-2.35(32)$	$-2.22(19)$
		119–125	69–75	$-(1.3 \div 2.6)$	$-2.02(21)$	
55	Cs	124–134	69–79	$-(2.2 \div 3.7)$	$-3.16(19)$	$-3.16(19)$
56	Ba	125–135	69–79	$-(1.8 \div 3.5)$	$-2.63(20)$	$-2.63(20)$
80	Hg	189–193	109–113	$-(2.2 \div 3.3)$	$-2.62(27)$	$-2.57(23)$
		199–203	119–123	$-(1.8 \div 3.4)$	$-2.54(40)$	

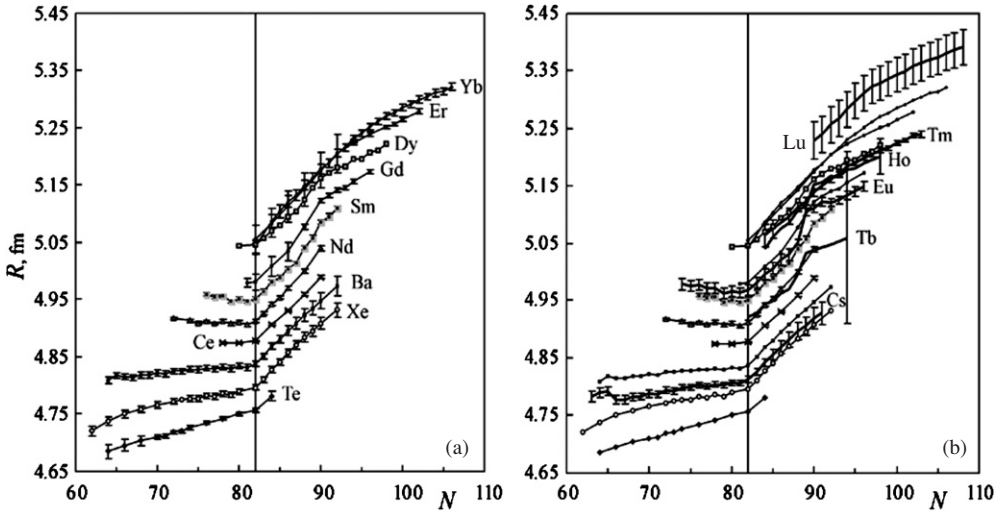

Figure 5. Isotopic behaviour of rms radii from Te to Lu with the error bars. (a) only the even-Z elements; and (b) the odd-Z elements Cs, Eu, Tb, Ho, Tm and Lu are added. For visual simplicity, the large uncertainties of the R-values for Ho and Tb are shown only for one isotope in the series. For the same reason, the uncertainties of about 0.2 fm in the case of Dy are not drawn.

In the region of light elements (figure 3), there are still large blank fields. So far, with an exception of very neutron deficient isotopes of Ne and Na, the $R(N)$-curves corresponding to larger Z are shifted towards higher R-values and the shifts are beyond the error limits.

4. Isotonic rms radii behaviour

The present investigation of rms nuclear charge radii over a broad range of elements and isotopes complements the earlier published results [2–4] and permits a more global survey not only of the isotopic but also of the isotonic radii development. According to [3], a smooth mass number dependence of the isotonic charge radii $R_N(Z)$ is described approximately by

$$R_N(A) = R_0 \left(\frac{A}{A_0}\right)^{1/2} \tag{4}$$

where R_0 is the rms charge radius of the reference isotone (N, A_0). The exponent in (4) exhibits a slight dependence on the neutron number (for details see [3, 18]). A striking difference is obvious from the comparison between equations (2) and (4): the slope of the isotonic curves, $R_N(Z)$, is considerably steeper than that of the isotopic curves, $R_Z(N)$. For the first time, this feature has been pointed out and discussed in connection with the radii around $Z = 50$ [14, 61] and can be understood in terms of the additional Coulomb interaction between protons compared to the interaction between neutrons.

Let us note that in the case of the isotonic radii trend one has to deal with a more complicated situation than for isotopic radii dependence. A principal difference exists as compared to the case of the isotonic series. Within an isotopic sequence—owing to optical isotope shift measurements—the relative accuracy of the R-values is nearly independent of the uncertainties of the source data on μ^- and e^- rms charge radii. Since in the isotonic sequences the R-values are composed of different elements, they inherit the errors both from the absolute R-values and from the isotope shifts that are built on the basic R'. Therefore, it is not reasonable to introduce relative uncertainties in the isotonic series in a way it was done in the isotopic series. This circumstance strongly affects the accuracy of the isotonic curves. In principle, the data along an isotonic series $R_N(Z)$ can also be tested quantitatively by introducing the corresponding second difference with a basic length $\Delta Z = 2$. However, the 'kink strength' values S exhibit very large errors (see the appendix, table A2) and the criterion of statistical significance $S \geqslant 3 \times \mathrm{d}S$ is fulfilled only in fewer cases. For this reason, only the global radii trend is conclusive while for different small radii changes there is a lack of confidence. Due to the steeper increase of charge radii in the isotonic sequences, even pronounced structural changes visually reflect in the isotonic charge radii behaviour less distinct than in the isotopic radii curves. Nevertheless, the peculiarities in the isotonic trends pose a challenge for theory. Some of those are pointed out below.

In addition, one should have in mind that an accidental use of an incorrect basic value R' from electronic scattering or muonic data may result in a dramatic change of the isotonic radii trend—producing false minima or maxima—and may lead to wrong conclusions. As already stressed in section 2, all the source data are carefully checked and even, if necessary, re-evaluated. This justifies a look over the general isotonic trend of R and its peculiarities (figure 6). Moreover, it is possible to arrive at some quantitative conclusions based on the S-values despite of the large uncertainties. This concerns predominantly the proton shell closures Z_M. As in the case of the isotopic chains, magic proton numbers Z_M are clearly associated with positive S-values exceeding well the uncertainties.

4.1. Series of light elements

In particular for the light elements, many new data on nuclear radii are collected allowing a more complete systematics of the charge radii in this region (figure 6(a)). Until now, the isotonic radii trend has been discussed only for nuclei around $Z = 20$ (calcium region) [35, 36]. Adding new data to and around this region clearly shows a situation different for the isotonic dependence in comparison to that for the isotopic dependence. Proton shell closures $Z_M = 8$ and $Z_M = 20$ are unambiguously evident in the isotonic radii development. Characteristic kinks at $Z = 8$ and 20 are observed like at any other major proton shell closure with $Z \geqslant 28$ (see figure 6(a)). This is also quantitatively confirmed by the S-values as can be seen in table A2 (see the appendix). Between the 'traditional' magic proton numbers $Z_M = 8$ (determined by $S(^{16}O_8) = 0.48(9)$ fm) and $Z_M = 20$, the slope of $R(Z)$ dependences develops from a steep increase at the beginning of the $\pi 2s1d$ shell and tends to saturate before $Z_M = 20$. For the double magic $^{48}Ca_{28}$, the kink strength reaches its maximum value and is nearly

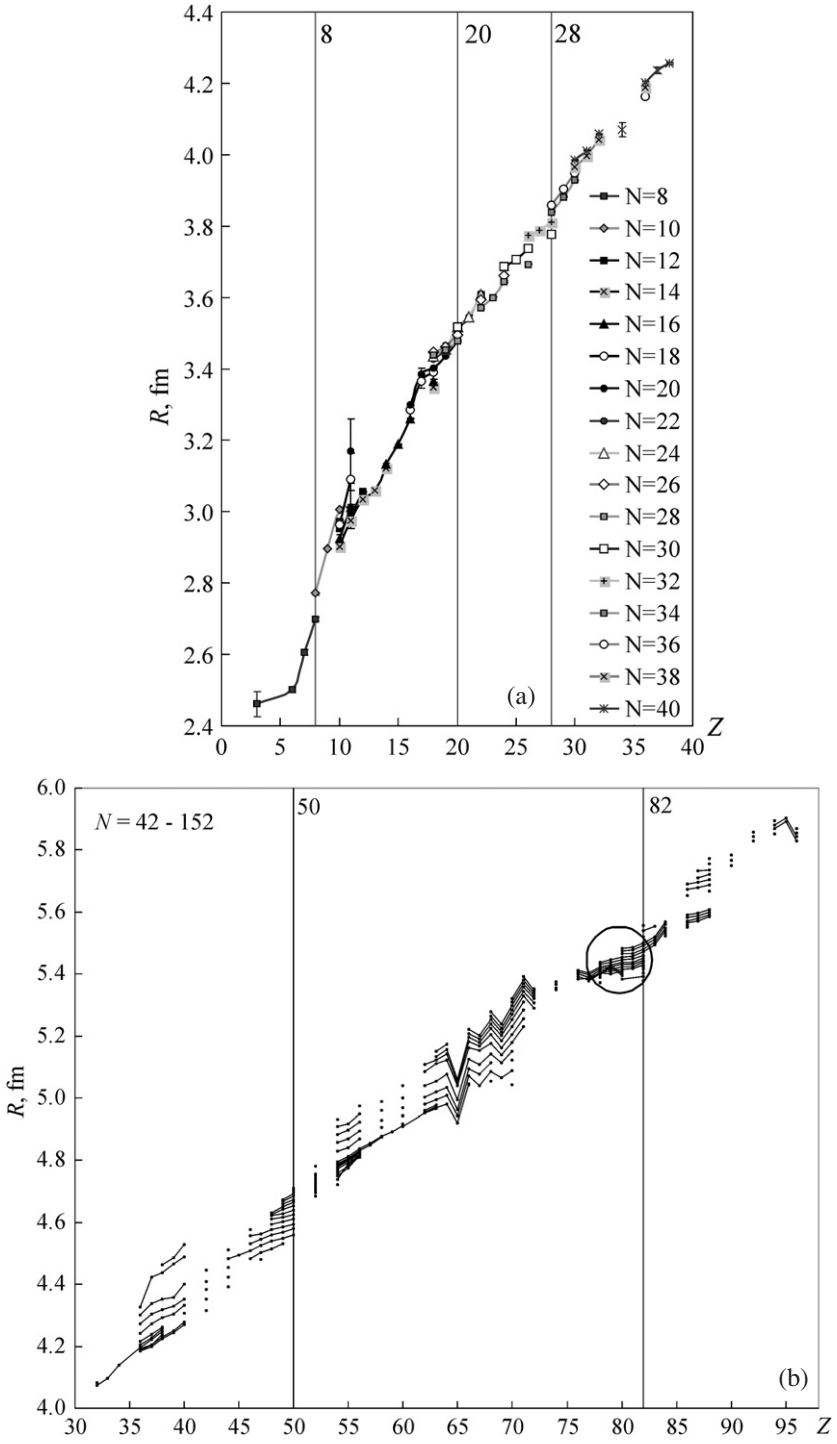

Figure 6. Isotonic behaviour of rms radii *R*. For visual simplicity only even *N* curves are drawn. The error bars shown in the case of light elements are usually within the limits of points. The few exceptions refer to the neutron-deficient isotopes of Ne and Na.

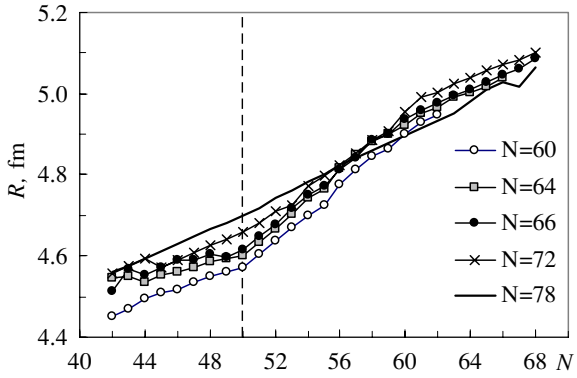

Figure 7. Isotonic trend of the rms charge radii around $Z = 50$ according the HFBSC-1 calculations [60].

the same in the isotonic and isotopic radii dependences: $S(^{48}\mathrm{Ca}) = 0.72(8)$ fm and 0.76(7) fm, respectively. With decreasing neutron number, S at $Z_\mathrm{M} = 20$ reduces strongly showing a tendency to vanish towards $N = 20$ (see table A2 and figure A2 in the appendix). Thus, the isotonic dependences supply additional evidence for the vanishing of the $N = 20$ shell effect with respect to nuclear charge radii.

Besides, other specific features are observed in this low Z region. For example, a characteristic change of slope at $Z = 6$ ($\pi 1\mathrm{p}_{3/2}$) for $N = 8$ appears. According to the systematics of [39] the nucleon pair $Z = 8$, $N = 6$ is identified as magic too. Unfortunately, we do not have data for any isotonic series at $N = 6$ and it is not possible to check whether the above statement holds for radii too. Due to the lack of enough data, it would also be early to draw definitive conclusions about radii behaviour at the possible proton shell closures at $Z < 8$.

Visually, the picture between proton magic numbers $Z_\mathrm{M} = 8$ and $Z_\mathrm{M} = 20$ is disturbed by a local 'dip' at $Z = 14$, indicating the magic-like behaviour at the closed $\pi\mathrm{d}_{5/2}$ subshell. This observation is consistent with the predictions of $Z = 14$ magicity [38, 39, 62, 63], but there are no sufficient data for a quantitative estimation of this fact using our S criterion.

4.2. Series of intermediate and heavy elements

As regards the isotonic behaviour at larger Z-values (figure 6(b)), the main features pointed out in [2] are valid. First, we will concentrate the attention on the magic numbers. Their influence on the isotonic radii trend causing a kink at Z_M is already underlined above. The kink strength for the magic proton number 50 varies from $S = 1.52(32)$ fm for $N = 64$ to $S = 0.73(15)$ fm for $N = 72$ (table A2). It is beyond doubt that S at $Z_\mathrm{M} = 50$ decreases steeply with increasing neutron number of the isotonic series (see figure A2, in the appendix). If an extrapolation towards larger N is made, one could suppose that in the region of neutron-rich nuclei the proton shell closure $Z_\mathrm{M} = 50$ is diminished. Such an effect follows from the HFBSC-1 calculations [60] too: at $Z_\mathrm{M} = 50$, $S = 1.17$ fm for $N = 64$; $S = 0.42$ fm for $N = 72$ but it decreases to $S = 0.25$ fm for $N = 78$ and the kink of the isotonic curves at the proton shell closure 50 disappears (figure 7).

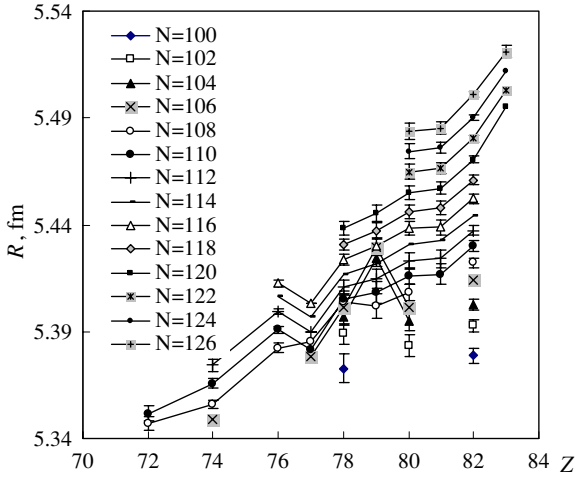

Figure 8. Trend of isotonic radii in the region of the intersection marked with a circle in figure 6(b). The very large errors (±0.1 fm) at $Z = 77$ covering a wide neutron range are not shown. An inverted sign of the OES at $Z = 79$ for $N < 108$ is observed.

Due to the use of estimated values of rms charge radii for the radioactive elements Po, Rn, Fr, Ra and Cm (for explanation see the caption of figure 4), the *S*-value at $Z_M = 82$ may not be correct. For this reason, it is neither included in table A2 nor discussed.

Regarding the magic numbers, several other large positive *S*-values should be considered too. These are the cases of $Z = 40$ and 64. The case of $Z = 40$ will be discussed separately in section 4.3. The kink strength $S \approx +1.6(70)$ fm for $_{64}$Gd isotopes with $N = 82$–86 is not included in table A2 because of the very large uncertainty. Thus, no quantitative argument based on the characteristics of the isotonic radii curves can be given, confirming earlier evidences that 64 might be a proton magic number [64, 65]. Instead, considering the low accuracy of the experimental *R*-values for elements in the near neighbourhood of $Z = 64$ ($Z = 64$–69), we would suggest improvement of the experimental data.

The remaining characteristics of the isotonic radii trend, similarity between the adjacent curves and the OES staggering [2], can be discussed only qualitatively. A striking feature of the isotonic systematics is that the curves for adjacent *N* are nearly parallel (see figure 6). This peculiarity seems to be more conspicuous than for the isotopic curves. The effect is due to the much steeper slope of the isotonic curves involving different proton numbers.

Next, the OES of the isotonic curves should be regarded. With few exceptions, it is a normal OES staggering causing a dip in the curve for odd *Z*. It is visible in figure 6 although the *R*-scale is very rough. A distinct OES is seen at $Z = 65$, 67, 69 and 77 (see also figure 8). It is to be noted that for these elements the charge radii uncertainties cover several isotonic curves (see e.g. figure 5(b)) and a quantitative description via *S*-factor fails. Thus, the apparently large OES may or may not be a real effect.

The (*Z*, *N*) region marked with a circle in figure 6(b) is worthy of closer consideration. It is presented in enlarged scales in figure 8. On average, the curves of different neutron numbers are well resolved. A characteristic peculiarity in figure 8 is the 'strange' behaviour of the Au radii at $N < 108$. The characteristics of the isotonic trend in the proton region 78–80 are more obvious from the presentation in figure 9. The 'inversion' of the odd–even staggering in the isotopic as well as in the isotonic radii sequences at $N < 108$ is clearly seen and the effect

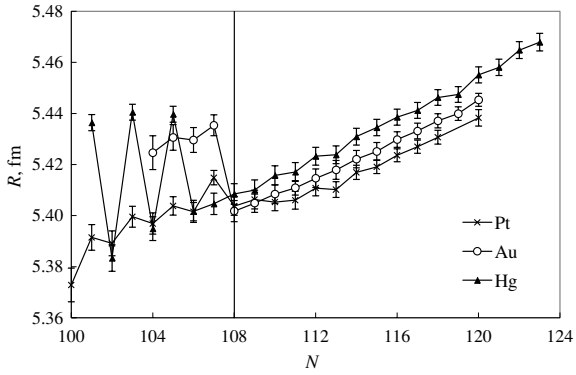

Figure 9. Neutron number dependence of the charge radii for the neighbouring elements Pt, Au and Hg. In the neutron-deficient region with $N < 108$, the sign of the odd–even staggering is inverted from negative (right) to positive (left) [14, 66, 67].

is far beyond the limits of the total, statistical plus systematic, uncertainties. Such behaviour can be explained by the influence of the odd proton which moves the Au isotopes over the more deformed prolate side of the potential energy surface. The effect is analogous to the inversion of the odd–even staggering observed in the mercury and platinum isotopes with $N < 108$. These cases are discussed many times (see e.g. [14] and the references therein, as well as more recent papers [53, 67–69]). The effect is ascribed to the competition between nearly spherical oblate (even isotopes) and most deformed prolate (odd isotopes) minima of the potential energy surface in the region with $N < 108$. The nuclei from the discussed Z, N region are soft and very sensitive to small perturbation caused by odd neutron or proton, and thus, the balance between both energy minima is very delicate.

4.3. Non-traditional magic numbers

A remarkable result of the experimental radii tabulation [7] is demonstrated in figure 10. It shows the $R(Z, N)$ dependence of the nuclear charge radii in a confined Z and N range. The local kink of the charge radii at $^{96}Zr_{56}$ is clearly seen. Returning to the S-values in tables A1 and A2, it is seen that a high positive S-value of 1.03(16) fm in the isotopic curve for $Z = 40$ and respectively of $S = 0.79(19)$ fm in the isotonic curve for $N = 56$ belong to the zirconium isotope $^{96}Zr_{56}$. This nucleus behaves as a double magic with both proton, $Z = 40$, and neutron, $N = 56$, non-traditional magic numbers. The effect is in overall agreement with other properties of this nucleus indicating that in addition to the major magic number $N = 50$, the neutron number $N = 56$ is also magic for zirconium [39, 70]. Figure 11 illustrates the vanishing quadrupole deformation β_2, the local maximum of the energy of the first 2^+ excited state $E_1(2^+)$ and the minimum of the ratio $E_1(4^+)/E_1(2^+)$ of the energies of the first $J^\pi = 4^+$ and $J^\pi = 2^+$ states at ^{90}Zr and at ^{96}Zr respectively (see [39]). Furthermore, a characteristic jump of the one and two neutron separation energies occurs at $N = 56$ [39, 71].

The subshell structure of the zirconium isotope ^{96}Zr exhibits corresponding peculiarities too. Stripping and pick-up experimental data as well as data on nuclear spins and parities have allowed deriving a picture on the shell evolution in the Zr isotopic sequence [70]. The energies and the occupancies of the subshells in ^{90,92,94,96}Zr have been obtained by a method [72] based on the sum rules for the spectroscopic factors. It was discovered that the energy gaps between the neutron $\nu 2d_{5/2}$ and $\nu 3s_{1/2}$ and the proton $\pi 2p_{1/2}$ and $\pi 1g_{9/2}$ orbitals in the

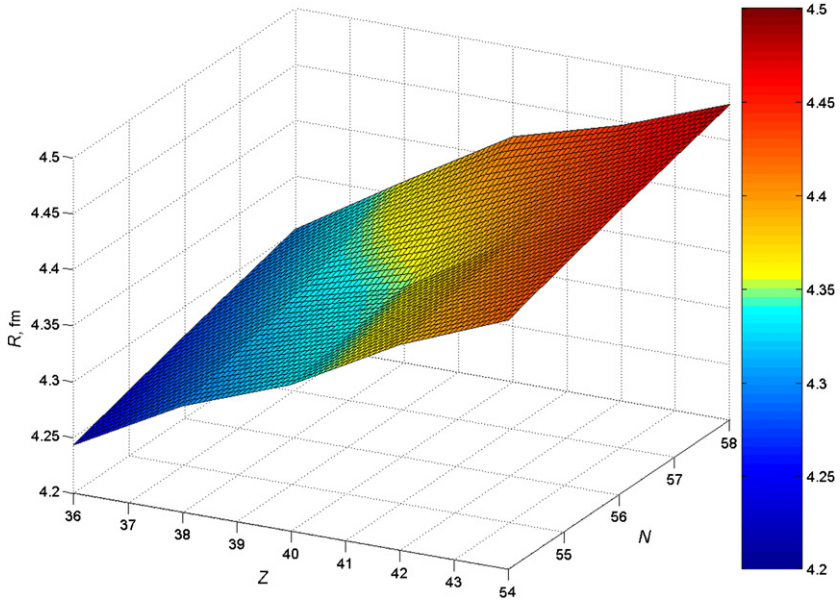

Figure 10. Charge radii dependence on Z and N in the range $36 \leqslant Z \leqslant 44$ and $54 \leqslant N \leqslant 58$.

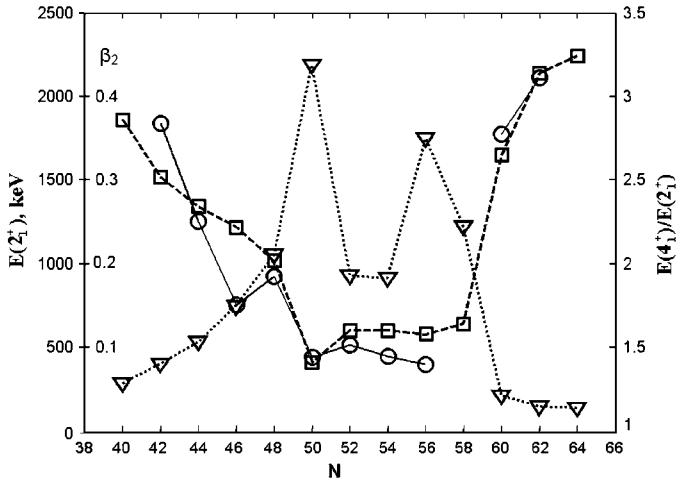

Figure 11. Energy of the first excited state $E_1(2^+)$ (∇) [29], ratio $E_1(4^+)/E_1(2^+)$ ($\square$) of the energies of the lowest 4^+ and 2^+ excited states [29] and quadrupole deformation β_2 ($\circ$) [28] in the isotopic sequence of Zr [39].

zirconium isotopes ^{90,92,94,96}Zr increase with increasing N and reach maximal values exactly at ^{96}Zr. The corresponding values are 2.3 MeV for the neutron gap and 3 MeV for the proton gap. In ^{96}Zr the $\nu 2d_{5/2}$ and the $\pi 2p_{1/2}$ orbitals are completely occupied. Therefore, in this isotope both neutron and proton subshell closures arise with significant energy gaps.

5. Nuclear charge radii in the theory—comparison with the experiment

This section is devoted to the comparison of the present results with up-to-date theoretical models. Note that there is a huge number of theoretical works which deal with nuclear parameters, including charge radii, of selected elements and in limited ranges of isotopes; some of these papers have already been referred above. However, in the context of this work a comparison with theories describing nuclear parameters *over a broad region* of nuclear masses and charges turns out to be more valuable. To our knowledge, these are the following: (i) the droplet model approach of [73] and its more global FRDM (finite range droplet model) version [74, 75]; (ii) microscopic Hartree–Fock approximation of [60, 76], in which the Skyrme force is fitted to the available mass data, with pairing correlations described by BCS or Bogolyubov methods and (iii) a self-consistent RMF (relativistic mean field) method with an effective Gogny interaction, the Skyrme energy functional, and the relativistic meson-exchange effective Lagrangian [77, 78]. The papers [60] and [77] are devoted not only to the construction of complete mass tables over the nuclide chart but also predict other measurable quantities not included in the original fits, e.g. rms nuclear charge radii.

Here a note on the proton radius is appropriate. Both tables calculate the rms charge radius for nuclei from the distribution of point-like protons by using $r_p = 0.8$ fm for the rms radius of the proton. However, the value $r_p = 0.805(11)$ fm was derived by [79] from the pioneering Stanford experiments. Since then, several improved measurements and analyses have been performed; here we mention the most important only. The result of the Mainz experiment [80] is significantly higher: $r_p = 0.862(12)$ fm. Worldwide data on electron–proton scattering have been re-analysed [81] taking into account corrections for Coulomb distortion and higher moments, resulting in $r_p = 0.895(18)$ fm. The evaluation of high-accuracy data of the 1S Lamb shift in hydrogen [82] yielded $r_p = 0.883(14)$ fm. The weighted average of these two data—measured by *independent methods*—is $r_{p,\mathrm{av}} = 0.887(11)$ fm. When constraints [3] from electron–deuteron scattering [83] and optical $\Delta r^2_{p,d}$ differences [84] are also taken into account, we arrive to $r_p = 0.879(9)$ fm. This is the value included in the last version of nuclear charge radii tables [5, 7].

The global rms deviation of 0.024 fm between HFBCS-1 theory [60] and experiment, including experimental rms charge radius data for 856 nuclei starting with $Z = 8$, is significantly better than 0.20 fm that was found by the RMF approach [77]. The latter describes the even–even isotopes only; therefore, in this case the comparison covers 327 double even nuclei for which experimental data are available. Note that unlike [85], no further parameter adjustment of [60] and [77] is used in this comparison. The rms charge radii not only exhibit a very good overall agreement with the predictions of the HFBSC-1 mass formula but also behave in many details as expected from this rather global model as already pointed out in sections 3 and 4.

There are some physically interesting features that are not reproduced. In the rare-earth region the similarity to the experimental data is predominantly qualitative. According to [60], no or a very small shell effect arises at $N = 82$ (figure 12), and the shape transition to strongly deformed rare-earth isotopes occurs at neutron numbers not corresponding to those well-established experimentally. In all cases, the curves at higher Z are shifted to larger R, opposite to the experimental trend shown in figure 5(b). An important example is the many times discussed 'kink' in the radii development at the double magic ^{208}Pb (see e.g. [14, 58, 85]). This problem does not exist in the RMF theory [77] which is particularly successful in describing both charge radii in the near-spherical Pb nuclei and radii in regions of the strong nuclear deformation, such as the Kr, Sr and Zr isotope chains. The ability of the RMF approach to reproduce the kink at the $N = 126$ shell is its notable achievement although the experimental data are generally overestimated (see figure 12).

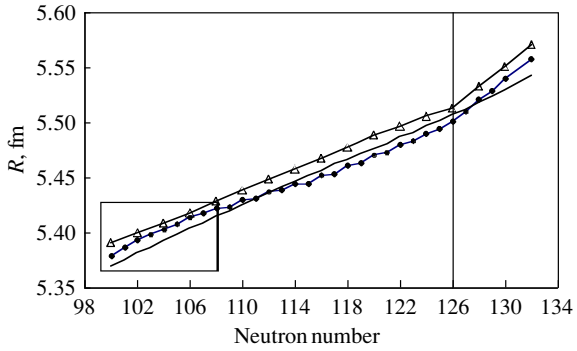

Figure 12. Charge radii in the Pb isotopic sequence. Comparison with theory: experimental data (black circles), RFM results [77] (triangles) and HFBCS-1 [60] data (full line). The updated experimental values cover a neutron number region extended towards the neutron-deficient isotopes. It is marked with a rectangle.

6. Summary

In conclusion, we will briefly summarize the main results of the present work. Due to the application of the ultra-high-sensitive laser spectroscopy techniques, isotopes far from stability have become accessible. Combined treatment of the isotope shift measurements in long isotopic series, including data up to the beginning of 2008, with the known absolute radii values from muonic and electron scattering experiments gives insight into the development of the rms charge radii over a broad range of neutron numbers for 76 elements from $_{1}$H to $_{96}$Cm. The accuracy of the data is high compared to the directly measured radii values for the same element. Thus, new information on the isotopic and isotonic behaviour of the nuclear charge radius is obtained.

Of special interest are the data concerning the light elements and the magic neutron and proton numbers in this region. The traditional proton magic numbers $Z = 8$, 20 and 28, as well as the neutron magic number $N = 28$, are evident from the charge radii development by a strong change in the curve slope. The neutron magic number $N = 20$ is violated in the case of the neutron-rich nuclei with Z around 10 and has no unambiguous confirmation for the stable nuclei from the Ca region. No experimental evidence is still available for the magicity of $N = 8$. Instead, there is a strong indication that $N = 6$ and N, $Z = 14$ may be magic or magic like. According to the charge radii development (see figure 6(a)), the (Z, N) pair (6, 8) should be regarded as double magic. There is also a vague indication for the magicity of the pair (2, 6) in figure 3. This experimental statement supports the new Brown and Richter [46] rule of double magic numbers. In the region of intermediate and heavy nuclei, special attention is paid to the appearance of a new non-traditional double magic nucleus ^{96}Zr.

This data analysis presents the *status quo* of our knowledge about the experimental values of the rms charge radii. Obviously, the experimental observation of the peculiarities in the isotopic and especially in the isotonic radii trends over the whole nuclide chart is of great potential to guide future investigations. Furthermore, the quantitative results provide important information which may serve as a guide to incorporate essential new features into the theoretical approaches.

Appendix A. The 'kink strength' *S*

Changes in the nuclear structure—as shell effects and deformation—give rise to changes, '*kinks*', in the mass number dependence of nuclear charge radii R. Along isotopic sequences,

Table A1. Kink strength values S in the isotopic dependence of charge radii.

Z	Element	A	N	S (fm)	ΔS (fm)	Z	Element	A	N	S (fm)	ΔS (fm)
2	He	6	4	−1.75	0.13	56	Ba	138	82	0.71	0.004
3	Li	9	6	1.90	0.32			139	83	0.26	0.007
10	Ne	20	10	−0.63	0.03	58	Ce	140	82	0.71	0.007
		23	13	0.61	0.10	60	Nd	141	81	0.58	0.03
		24	14	0.63	0.07			142	82	0.74	0.02
11	Na	25	14	0.46	0.10			143	83	0.23	0.03
20	Ca	42	22	−0.25	0.02			148	88	0.28	0.03
		43	23	−0.22	0.02	62	Sm	141	79	0.22	0.03
		44	24	−0.40	0.03			143	81	0.50	0.02
		48	28	0.76	0.07			144	82	0.79	0.03
22	Ti	47	25	−0.32	0.04			148	86	0.46	0.15
24	Cr	52	28	0.87	0.08			149	87	0.65	0.18
34	Se	76	42	−1.23	0.36	63	Eu	142	79	0.25	0.05
36	Kr	76	40	−0.23	0.02			143	80	0.24	0.03
		85	49	0.32	0.02			144	81	0.48	0.05
		86	50	0.75	0.01			145	82	0.69	0.05
		87	51	0.32	0.02			150	87	1.47	0.25
37	Rb	78	41	−0.44	0.06			151	88	0.77	0.09
		83	46	0.27	0.01			152	89	−1.73	0.23
		84	47	0.38	0.02			153	90	−1.41	0.02
		86	49	0.25	0.02	64	Gd	154	90	−0.69	0.003
		87	50	0.95	0.01			156	92	−0.14	0.004
		88	51	0.51	0.04	65	Tb	152	87	1.31	0.15
		95	58	1.11	0.08			155	90	−1.00	0.08
		96	59	1.18	0.08	66	Dy	148	82	0.62	0.07
38	Sr	85	47	0.20	0.02	67	Ho	155	88	0.38	0.04
		87	49	0.46	0.01			156	89	0.54	0.04
		88	50	0.95	0.01			157	90	−0.91	0.02
		89	51	0.39	0.01			158	91	−1.03	0.03
		96	58	1.21	0.04	69	Tm	163	94	−0.23	0.02
		97	59	1.28	0.04	70	Yb	167	97	−0.24	0.021
		98	60	−1.39	0.06	71	Lu	167	96	−0.29	0.009
39	Y	88	49	0.40	0.11			168	97	−0.36	0.008
40	Zr	89	49	0.47	0.02	72	Hf	175	103	0.21	0.06
		90	50	0.95	0.05			180	108	−0.24	0.04
		96	56	1.03	0.16	77	Ir	185	108	−0.38	0.03
		98	58	0.69	0.08			186	109	−0.51	0.03
		99	59	1.48	0.03			187	110	0.42	0.03
		100	60	−1.19	0.03	78	Pt	180	102	−0.28	0.09
42	Mo	98	56	0.26	0.07			183	105	0.28	0.07
48	Cd	116	68	−0.22	0.03			185	107	−0.66	0.08
54	Xe	136	82	0.77	0.010	79	Au	185	106	−1.10	0.07
55	Cs	120	65	−0.54	0.010			186	107	−1.15	0.07
		121	66	0.43	0.016			187	108	1.17	0.06

Table A1. (Continued.)

Z	Element	A	N	S (fm)	ΔS (fm)	Z	Element	A	N	S (fm)	ΔS (fm)
		122	67	0.48	0.009			188	109	1.20	0.06
		136	81	0.44	0.009	80	Hg	185	105	−1.14	0.02
		137	82	0.61	0.007			187	107	1.35	0.02
		138	83	0.27	0.007	82	Pb	208	126	0.31	0.03
56	Ba	123	67	0.21	0.017	87	Fr	225	138	0.23	0.018
		137	81	0.49	0.007			226	139	0.29	0.019

Table A2. Kink strength values S in the isotonic dependence of charge radii.

N	A	Z	S (fm)	ΔS (fm)	N	A	Z	S (fm)	ΔS (fm)
8	16	8	0.48	0.09	54	94	40	0.42	0.14
14	26	12	−0.38	0.08	55	97	42	−0.58	0.19
16	32	16	−0.24	0.07	56	96	40	0.79	0.19
20	38	18	−0.33	0.05		98	42	−0.30	0.09
22	42	20	0.28	0.09	64	114	50	1.52	0.32
23	43	20	0.35	0.07	66	116	50	1.47	0.27
25	45	20	0.54	0.08	68	118	50	1.31	0.24
26	46	20	0.61	0.08	70	120	50	0.90	0.14
	48	22	−0.37	0.07	72	122	50	0.73	0.15
28	48	20	0.72	0.08	101	181	80	−3.15	0.28
	50	22	−0.30	0.07	103	183	80	−2.80	0.26
	52	24	−0.30	0.07	105	185	80	−2.33	0.25
40	72	32	−1.05	0.35					
	74	34	2.11	0.71					
	76	36	−1.36	0.39					

these small variations in the slope of $R_Z(N)$ series can be observed easily by investigating the second difference $\mathrm{d}^2R/\mathrm{d}N^2$. In order to eliminate the effect of odd–even staggering, $\mathrm{d}N = 2$ intervals were used to calculate the differences $\mathrm{d}R$. This results in an increase of the peak width to $\mathrm{d}N = 2$, and in the loss of the first and last two points in the isotopic chain. A nucleon added to a heavy nucleus produces a smaller radius increase than that added to a light nucleus, as it is distributed on a larger surface. This trivial mass number dependence can be compensated by multiplying the radius difference by $A^{2/3}$. Therefore, in what follows, the slope change, *kink*, will be characterized by the quantity

$$S_Z(N) = \frac{\mathrm{d}^2 R_Z(N)}{\mathrm{d}(2N)^2} \times A^{2/3}. \tag{A.1}$$

The *kinks* in the isotonic sequences can be defined in an analogous way by simply exchanging N and Z in equation (A.1). In the main text the short form S will be used, where the subscript and argument are not necessary.

Numerical values of significant S-values are given in tables A1 (isotopic series) and A2 (isotonic series). Here significance means that the absolute value of S is higher than the limit 0.2 (isotopic series) and higher than three times (isotonic series) its error, i.e. if $|S| > 0.2$, and $|S| > 3 \times \Delta S$. It should be noted here that in calculating the uncertainties ΔS, the relative ΔR_{rel} errors are used for isotopic series, which are derived mainly from OIS measurements, while

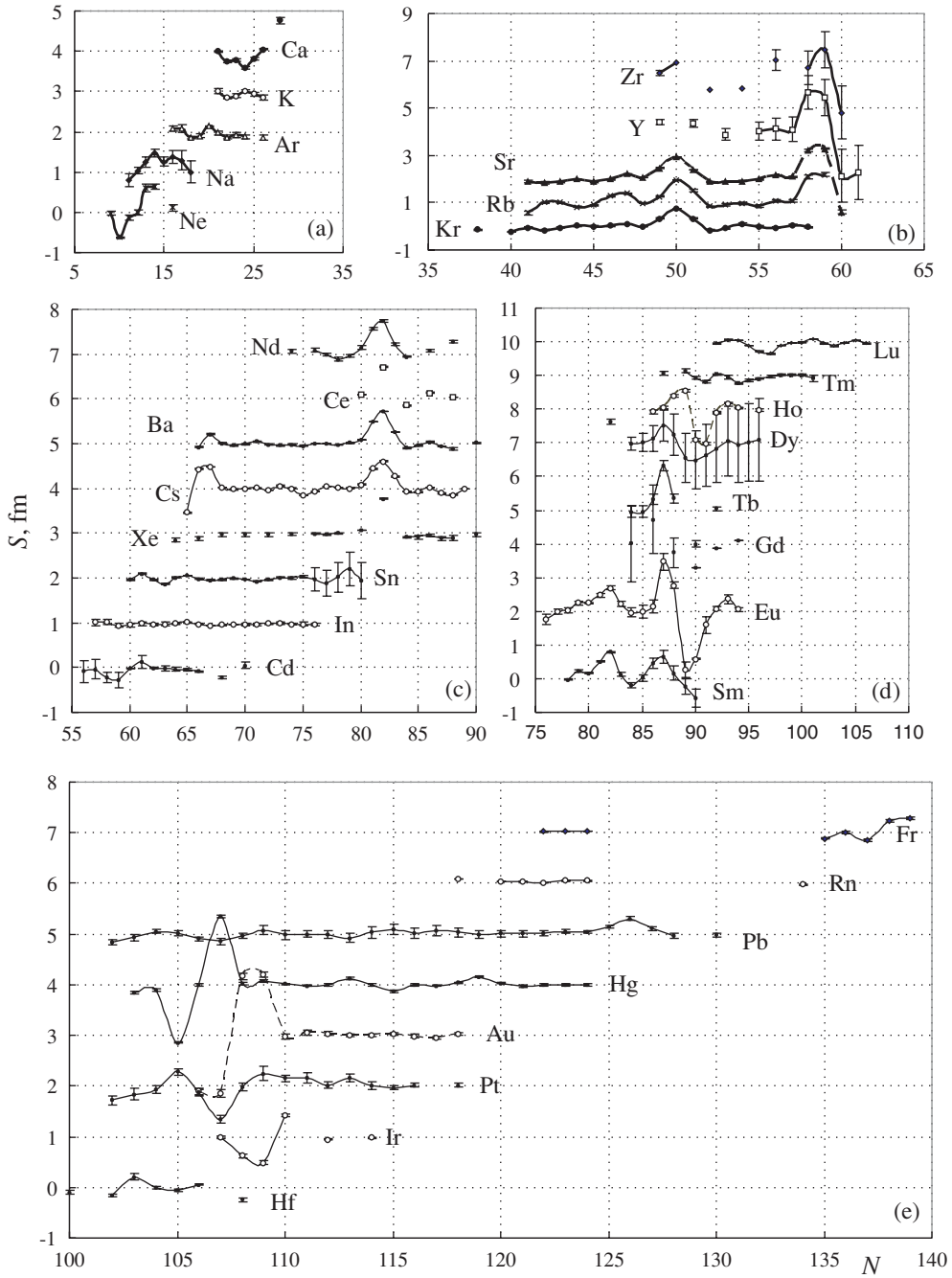

Figure A1. Trends of the kink strength in several isotopic series. To prevent confusing with the different series, they are shifted vertically by integer units in S (see also the identification symbols). Note isolated points.

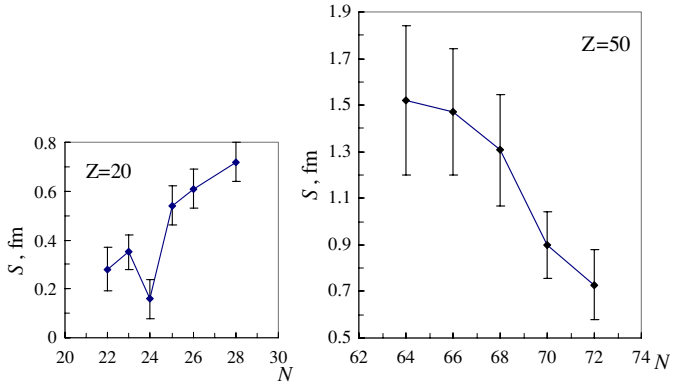

Figure A2. Neutron number dependence of the kink strength at the magic proton numbers 20 and 50.

total errors $\Delta R_{\rm tot}$ are taken into account in the case of isotonic series, where all experimental methods contribute to the R-values.

To illustrate the situation, a graphical presentation of some results is given. Figures A1(a)–(e) display the neutron number dependence of S in the isotopic sequences of several elements, i.e. $S_Z(N)$. Figure A2 shows the N dependence of S at the magic proton numbers $Z_{\rm M} = 20$ and $Z_{\rm M} = 50$ as follows from the isotonic sequences, i.e. $S_N(Z)$ at $Z =$ constant. Physical conclusions are discussed in the main text.

References

[1] Angeli I 1999 Table of nuclear root mean square charge radii INDC(HUN)-033 (IAEA Nuclear Data Section, Vienna)
[2] Nadjakov E G, Marinova K P and Gangrsky Yu P 1994 *At. Data Nucl. Data Tables* **56** 133
[3] Angeli I 2004 *At. Data Nucl. Data Tables* **87** 185
[4] Fricke G and Heilig K 2004 *Nuclear Charge Radii (Landolt–Börnstein: Numerical Data and Functional Relationships in Science and Technology New Series: Group I: Elementary Particles, Nuclei and Atoms)* vol 20 ed H Schopper (Berlin: Springer)
[5] Angeli I 2008 Recommended values of nuclear charge radii http://cdfe.sinp.msu.ru/services/radchart/radhelp.html#rad
[6] Gangrsky Yu and Marinova K 2008 Nuclear charge radii http://cdfe.sinp.msu.ru/services/radchart/radhelp.html#rad
[7] Database of the Lomonosov Moscow State University, Skobeltsyn Institute of Nuclear Physics http://cdfe.sinp.msu.ru/services/radchart/radmain.html
[8] Fricke G *et al* 1995 *At. Data Nucl. Data Tables* **60** 177
[9] King W H 1984 *Isotope Shift in Atomic Spectra* (New York: Plenum)
[10] Libert J *et al* 2007 *Nucl. Phys.* A **786** 47
[11] Silverans R E *et al* 1988 *Phys. Rev. Lett.* **60** 2607
[12] Keim M *et al* 1995 *Nucl. Phys.* A **586** 219
[13] Buchinger F *et al* 1990 *Phys. Rev.* C **41** 2883
[14] Otten E W 1989 *Treatise on Heavy-Ion Science* vol 8 ed D A Bromley (New York: Plenum) p 517
[15] Blundell S A *et al* 1985 *Z. Phys.* A **321** 31
[16] Anselment M *et al* 1986 *Nucl. Phys.* A **451** 471
[17] Billowes J and Campbell P 1995 *J. Phys. G* **21** 707
[18] Angeli I 2005 *Acta Univ. Debrecen, Ser. Phys. Chem.* **38-39** 21
[19] Kopfermann H 1958 *Nuclear Moments* (New York: Academic)
[20] Stacey D N 1966 *Rep. Prog. Phys.* **291** 171
[21] Angeli I and Csatlós M 1977 *Nucl. Phys.* A **288** 480

[22] Nörtershäuser W *et al* 2009 *Phys. Rev. Lett.* **102** 062503
[23] Geithner W *et al* 2008 *Phys. Rev. Lett.* **101** 252502
[24] Zhukov M and Thompson I 1995 *Phys. Rev.* C **52** 3505
[25] Nakamura S *et al* 1998 *Phys. Lett.* B **416** 1
[26] Huber G *et al* 1978 *Phys. Rev.* C **18** 2342
[27] Touchard F *et al* 1982 *Phys. Rev.* C **25** 2756
[28] Raman S, Nestor C W Jr and Tikkanen P 2001 *At. Data Nucl. Data Tables* **78** 1
[29] Evaluated Nuclear Structure Data File (http://www.nndc.bnl.gov/21/)
[30] Keim M *et al* 2000 *Eur. Phys. J.* A **8** 31
[31] Yanagisawa Y *et al* 2004 *Nucl. Phys.* A **734** 374
[32] Neyens G *et al* 2005 *Phys. Rev. Lett.* **94** 022501
[33] Warburton E K *et al* 1990 *Phys. Rev.* C **41** 1147
[34] Klein A *et al* 1996 *Nucl. Phys.* A **607** 1
[35] Blaum K *et al* 2006 *Hyperfine Interact.* **162** 101
[36] Blaum K *et al* 2008 *Nucl. Phys.* A **799** 30
[37] Casten R F *et al* 1987 *Phys. Rev. Lett.* **58** 658
[38] Angeli I 1991 *J. Phys. G* **17** 439
[39] Boboshin I N 2008 Classical and new magic nuclei *Preprint MSU SINP* (Moscow) N2008-7/843
[40] Iwasaki H *et al* 2000 *Phys. Lett.* B **481** 7
Iwasaki H *et al* 2000 *Phys. Lett.* B **491** 8
[41] Navin A *et al* 2000 *Phys. Rev. Lett.* **85** 266
[42] Otsuka T *et al* 2001 *Phys. Rev. Lett.* **87** 082502
[43] Jha T K *et al* 2003 *Pramana J. Phys.* **61** 517
[44] Stanoiu M *et al* 2004 *Phys. Rev.* C **69** 034312
[45] Becheva E *et al* 2006 *Phys. Rev. Lett.* **96** 012501
[46] Brown B A and Richter W A 2005 *Phys. Rev.* C **72** 057301
[47] Kowalewska D *et al* 1991 *Phys. Rev.* A **44** R1442
[48] Thibault C *et al* 1981 *Phys. Rev.* C **23** 2720
[49] Campbell P *et al* 2002 *Phys. Rev. Lett.* **89** 082501
[50] Cheal B *et al* 2007 *Phys. Lett.* B **645** 133
[51] Thibault C *et al* 1981 *Nucl. Phys.* A **367** 1
[52] Verney D *et al* 2006 *Eur. J. Phys.* A **30** 489
[53] Passler G *et al* 1994 *Nucl. Phys.* A **580** 173
[54] de Witte H *et al* 2007 *Phys. Rev. Lett.* **98** 112502
[55] Lievens P *et al* 1996 *Europhys. Lett.* **33** 11
[56] Le Blanc F *et al* 1999 *Phys. Rev.* C **60** 054310
[57] Regge U and Zawischa D 1988 *Phys. Rev. Lett.* **61** 149
[58] Rebel H 1988 *Recent Advances in Nuclear Physics* ed M Petrovici and N V Zamfir (Singapore: World Scientific) p 223
[59] Holbrow S H *et al* 1991 *Nucl. Instrum. Methods Phys. Res.* B **56/57** 528
[60] Goriely S, Tondeur F and Pearson J M 2001 *At. Data Nucl. Data Tables* **77** 311
[61] Buchinger F *et al* 1987 *Nucl. Phys.* A **462** 305
[62] Uno M and Yamada M 1981 *Prog. Theor. Phys.* **65** 1322
[63] Samanta C *et al* 2002 *Phys. Rev.* C **65** 037301
[64] Ogawa M *et al* 1978 *Phys. Rev. Lett.* **41** 289
[65] Casten R F *et al* 1981 *Phys. Rev. Lett.* **47** 1433
[66] Wallmeroth K *et al* 1989 *Nucl. Phys.* A **493** 224
[67] Hilberath Th *et al* 1992 *Z. Phys.* A **342** 1
[68] Le Blanc F *et al* 1997 *Phys. Rev. Lett.* **79** 2213
[69] Le Blanc F 2000 *Hyperfine Interact.* **127** 71
[70] Boboshin I N *et al* 2004 *Phys. At. Nucl.* **67** 1846
[71] Audi G, Wapstra A H and Thibault C 2003 *Nucl. Phys.* A **729** 337
[72] Boboshin I N *et al* 1989 *Nucl. Phys.* A **496** 93
[73] Myers W D and Schmidt K H 1983 *Nucl. Phys.* A **410** 61
[74] Möller P *et al* 1988 *At. Data Nucl. Data Tables* **39** 225
[75] Möller P *et al* 1995 *At. Data Nucl. Data Tables* **59** 185
[76] Goriely S *et al* 2003 *Phys. Rev.* C **68** 054325
[77] Lalazissis G A, Raman S and Ring P *1999 At. Data Nucl. Data Tables* **71** 1

[78] Lalazissis G A *et al* 2005 *Phys. Rev.* C **71** 024312
[79] Hand L N, Miller D G and Wilson R 1963 *Rev. Mod. Phys.* **35** 335
[80] Simon G G *et al* 1980 *Nucl. Phys.* A **333** 381
[81] Sick I 2003 *Phys. Lett.* B **576** 62
[82] Melnikov K and van Rittbergen T 2000 *Phys. Rev. Lett.* **84** 1673
[83] Sick I and Trautmann D 1998 *Nucl. Phys.* A **637** 559
[84] Huber G *et al* 1998 *Phys. Rev. Lett.* **80** 468
[85] Buchinger F, Pearson J M and Goriely S 2001 *Phys. Rev.* C **64** 067303